Chapter 8

SPECTROPHOTOMETRIC MEASUREMENT TECHNIQUES OF WEAK EMISSIONS IN TWILIGHT AIRGLOW

Craig A. Tepley
National Astronomy and Ionosphere Center, Arecibo Observatory,
P. O. Box 995, Arecibo, PR 00613

SUMMARY

The measurement of weak spectral lines during twilight requires a careful analysis treatment for the removal of scattered solar Fraunhofer structure. We first describe the process of resonant scattering and discuss the geometry encountered during a twilight experiment, including the effects of the transmission of the lower atmosphere to the excitation radiation. This is followed by a description of an analysis procedure which stresses the need to account for an additional continuum other than the measured solar and nightglow spectra. Some observations of the temporal and spectral behavior of this extra continuum are also given.

1. INTRODUCTION

Twilight is by definition that period just after sunset and before sunrise when a portion of the atmosphere is illuminated by the sun's rays from below, contrary to daylight when the rays enter the atmosphere from above. As the solar zenith, or depression angle increases, the lower atmosphere becomes progressively darker as the rays from the sun continue to rise in the atmosphere. This condition permits a variety of structure and composition studies of many minor constituents of the atmosphere by measuring their scattered resonant or fluorescent radiation from the sun. As the strong scattered light from the solar continuum decays, observations from the ground of the weaker resonance lines of many species are feasible, compared to what would otherwise be an impossible task in daylight. In the absence of solar illumination at night the measurement of species through their resonant excitation is also impossible unless an artificial source such as a lidar is employed.

Although somewhat limited in the range of the species that can be observed, ground-based optical observations using spectrophotometric techniques during twilight offer an inexpensive means to study the minor constituents of the middle atmosphere compared with rocket observations. For a particular region of the atmosphere, for example between 50 to 150 km altitude, twilight may last for several hours in the polar regions but only 15 or 20 minutes near the equator, depending on the season. Even during short twilights if sufficiently fast data sampling techniques are employed, such as programmable wavelength scanning spectrometers [Meriwether, 1979], and with knowledge or good estimates of the transmission of the atmosphere to the excitation energy, the inversion of the scattered emission profile will yield reasonable estimates of the altitude distribution of the species under study. Nevertheless, except for only a few cases, this powerful technique has not been fully exploited since the pioneering work that was accomplished in the 60's.

It is not the purpose of this report to provide a complete and exhausted review of all twilight measurements that have been made to date. We regret any omissions that would otherwise deserve proper reference. We will try to outline, however, some of those accomplishments with particular emphasis on investigations of the middle atmosphere, where future efforts would play important roles in understanding the chemistry and dynamics of that region, and which are an important part of the WITS program with regard to composition studies. Next, we offer a brief description of the observational method used to acquire spectral information, first through a synopsis of the scattering process followed by the experimental geometry encountered in twilight. The paper concludes with a detailed discussion of the data reduction techniques needed for the analysis of the spectra obtained, and of the relevant errors involved. Emphasis is placed on the need to account for a quasi-continuum in the analysis which may be the result of a lingering fluorescence of aerosols from the lower atmosphere during the twilight periods, and which can seriously affect the ability to obtain accurate magnitudes of weak line emissions.

2. OBSERVATIONS

Hunten [1967] gave a very thorough account of twilight airglow studies that occurred before the late 60's. He discussed several of the nightglow emissions that were observed to have twilight enhancements, and summarized those which can only be measured during twilight periods. Some notable examples of these include the thermospheric emissions of the first negative band system of N_2^+ [Lytle and Hunten, 1962; Broadfoot and Hunten, 1966], the metastable states of $O(^1D)$ and $N(^2D)$ [Barbier, 1959; Noxon, 1964; Dufay, 1953], and the infrared $He(^3P)$ line at 1.08 μm [Fedorova, 1961]. Emissions from the lower thermosphere which can be observed in twilight include the atmospheric and infrared atmospheric bands of O_2 [Vallance Jones and Harrison, 1958] and the resonant lines of various metallic atoms and ions, in particular those from the alkali metals [Broadfoot, 1967; Chamberlain, 1961; Gadsden, 1969; see also Hunten, 1967].

In the two decades following the earlier work briefly outlined above, there have been only a few ground-based twilight measurements of emissions from the upper ionosphere and thermosphere. These are the observations of $O^+(^2P)$ [Meriwether et al., 1978], the emissions from the metastable ^1S and ^1D states of N^+ [Torr et al., 1981; 1983], and more recently of N_2^+, an example of which is shown in Figure 1 [Torr et al., 1989]. Twilight enhancements have been observed from balloons and from the ground for the (0-1) component of both the molecular oxygen bands mentioned above [Evans et al., 1970; Pick et al., 1971; Noxon, 1975; Lowe et al., 1984]. The enhancement arises from both fluorescent scattering of sunlight and from photochemistry, the latter of which can provide estimates of the ozone concentration below about 100 km [Evans and Llewellyn, 1972; Noxon, 1975].

The presence of metallic species in the lower ionosphere from about 70 to 125 km can provide important tracers of the dynamics and chemistry of that region. However, very few attempts have been made during the last twenty years with ground-based observations using resonant scattering from the sun in twilight in order to investigate

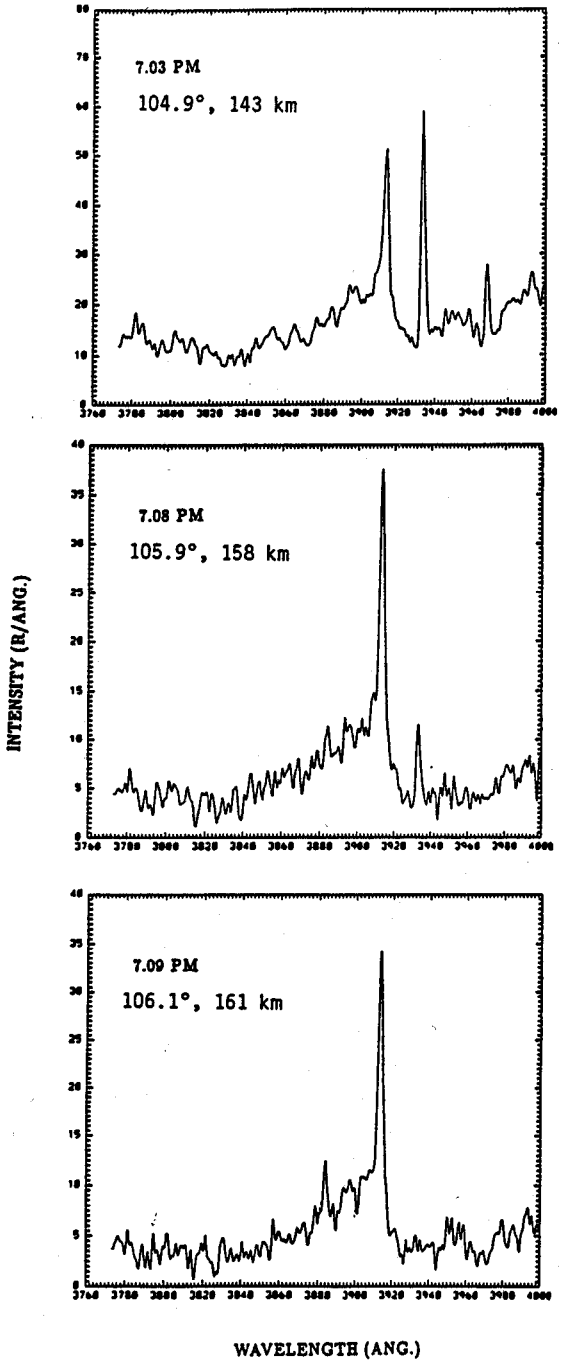

Figure 1 - Three twilight spectra measured on the evening of 22 December 1987 by Torr et al. [1989] showing the rotational distribution of the (0-0) and (1-1) bands of the N_2^+ 1st Negative system at 3914Å and 3884Å, respectively, and the appearance of the H and K lines of Ca^+ at 3968Å and 3934Å. (Figure courtesy of D.G. Torr).

the behavior of these metals. There have been a few polar and equatorial observations of Li and Na [Henriksen et al., 1980; Kirchhoff and Clemesha, 1973], and those of Fe and Ca^+ from low and mid-latitudes sites [Broadfoot and Johansen, 1976; Tepley et al., 1981a,b; Torr et al., 1989]. Observations of a metal in both its neutral and ionic form will help unravel the chemical distribution of these species. The ionic states of the more abundant metals as measured by mass spectrometers using rockets, such as Fe^+, Mg^+, and Ni^+, have resonance lines in the ultraviolet. Unfortunately, the lesser abundant calcium is the only metal which can be observed from the ground as both Ca and Ca^+. Although somewhat rare in occurrence, one such twilight detection for example, of the resonant emission from neutral calcium at 4227Å is shown in Figure 2. The progressive decay of the strength of this line with increasing solar depression angle can be compared with the average variations of similar observations of Ca^+ made from the same location [see figure 2 of Tepley et al., 1981b]. Ratios of the derived concentrations, that is $[Ca^+]$ / [Ca], (or column abundances) range from 0.7 near 91 km to 3.0 at 98 km altitude, which are consistent with chemical models of these metals in this altitude region [Brown, 1973].

Spectroscopic measurements of weak emissions in twilight with ground-based instruments is a powerful tool to study the composition of the atmosphere. Future observations can still take advantage of this useful and relatively inexpensive technique. The method, however, has been eclipsed in the last ten years by more powerful lidar remote sensing of the metals, in particular in detailed investigations of the alkalis [Megie et al., 1978; Clemesha, 1984; Gardner and Shelton, 1985], but also more recently with measurements of Fe, Ca, and Ca^+ [Granier et al., 1989a,b]. Lidar studies are not necessarily restricted to nighttime observations but can also be made during the day [Granier and Megie, 1982; Kwon et al., 1987]. The technique lends itself, not only to the composition studies mentioned above, but to direct measurements of the temperature of the mesopause region [Fricke and von Zahn, 1985; von Zahn and Neuber, 1987].

3. SPECTROSCOPIC BACKGROUND

Here we outline some of the basic spectroscopic theories encountered. Much of what we describe with regard to resonant scattering is detailed in two excellent texts by J.W. Chamberlain, *Physics of the Aurora and Airglow* and *Theory of Planetary Atmospheres*. The former text is almost 30 years old but is still a very useful standard reference for all aspects of airglow and auroral studies. The notation used in the rest of this section is similar, and in many ways identical, to that found in Chamberlain's texts.

The process of resonant scattering in an optically thin atmosphere will be treated first. This is the simplest form of scattering ignoring such effects as multiple scattering or the deactivation of the scatterers before emission occurs, otherwise known as quenching. When the atmosphere is considered optically thick, that is, the intensity of the emission is strong while the concentration of the emitters is large, the equations are still tractable. However, for weaker lines, such as metallic radiations in twilight for example, this is not the case (that is, optically thin conditions prevail) and we will show that the simple theory is valid. In the following section the additional problems

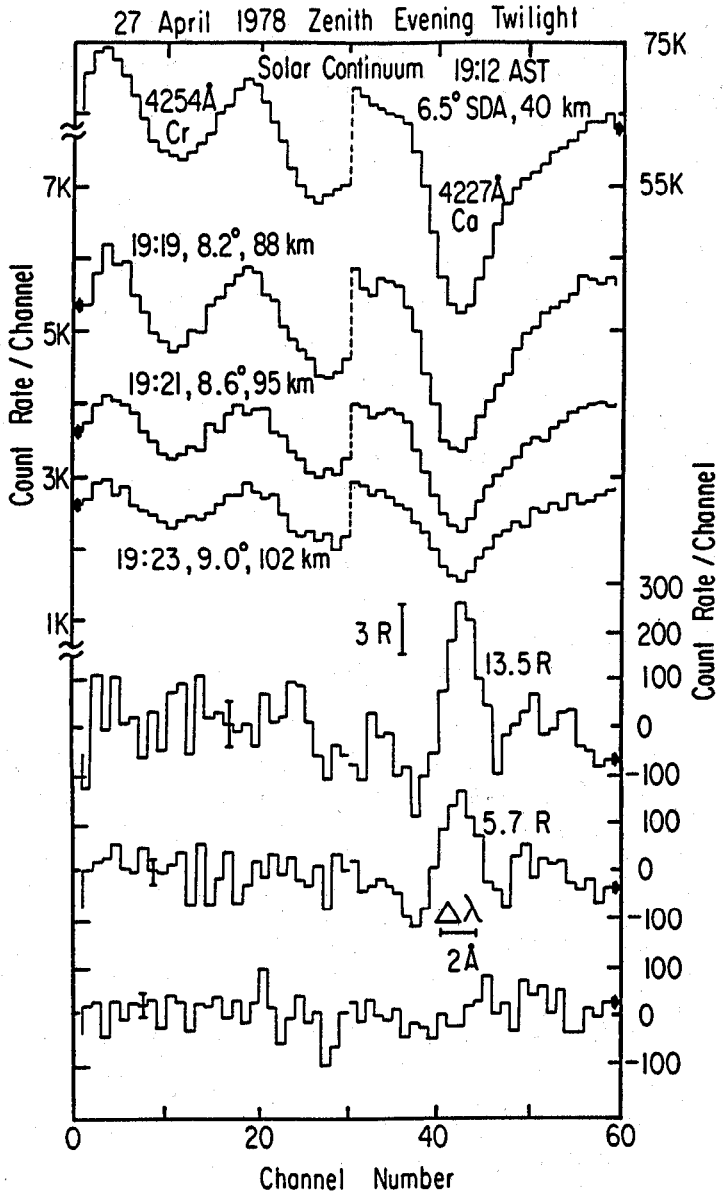

Figure 2 - Detection of the Ca(4227Å) resonance line in the evening twilight of 27 April 1978. The top spectrum is the scattered solar continuum measured in early twilight showing the Ca and Cr(4254Å) Fraunhofer absorption features. A programmable wavelength scan was used to obtain these spectra over two short ranges near the resonance lines of these metals [see Meriwether, 1979]. The next three spectra shown below the solar continuum were measured from middle twilight between about 8° and 9° solar depression. The bottom three curves are the results of applying the data reduction technique described in Section 5 to the middle twilight spectra, showing the detection of Ca and the absence of the Cr resonance.

encountered when dealing with resonant emissions are also discussed. These include the effects of atmospheric absorption and secondary scattering of both the incident and radiated energies, generally called extinction, and the atmospheric screening and transmission of the radiation. We can view these extra effects as an extension to the simply theory.

3.1 Resonant scattering

Before we describe the governing equations characteristic of resonant scattered emissions, we first outline some basic concepts of airglow photometry. In photometric studies it is usually common to express the surface brightness of some distant source in units of erg cm^{-2} s^{-1} str^{-1}. In airglow and auroral work the energy unit is replaced with the number of photons for convenience. If the source at a distance r from the observer is characterized by a volume emission rate given by E(r) photons cm^{-3} s^{-1}, then integrating with respect to the column distance yields its surface brightness, or

$$4\pi I = \int_o^\infty E(r)\, dr \tag{3.1}$$

where $4\pi I$ has the units photons cm^{-2} s^{-1}. This leads to the concept of the Rayleigh. If I has the units of 10^6 photons cm^{-2} s^{-1} str^{-1}, then $4\pi I$ is equal to one rayleigh (R) emission.

Resonance scattering of solar radiation is a convenient way of identifying certain atoms and molecules. The resonance lines of these species can be thought of as their fingerprint, and are usually identified by the transitions from the lowest lying excited energy level to the ground state of the species. Resonance emission is distinguished from fluorescence in that the absorbed solar energy is reradiated at the same frequency. Fluorescence is energy reradiated by a route within the energy levels of an atom or molecule which is different from the absorption path. Consider a situation where solar radiation is uniformally scattered by a collection of atoms. If there is no deactivation of the resonant energy through collisions before reradiation, then for a solar flux per unit area at a frequency ν penetrating to an altitude z is given by $\pi F_\nu(z)$, the energy absorbed is $\pi F_\nu(z) n(z) \alpha_\nu$, where n(z) is the number density of atoms at height z which are in their ground state and α_ν is the absorption coefficient. The absorption coefficient for a particular state of an atom is related to the transition probability A and the statistical weight $\tilde{\omega}$ of that state. Summing over all frequencies we have

$$\int \alpha_\omega(0,1)\, d\nu = \frac{\pi e^2}{m_e c}\ f(0,1) = \frac{c^2}{8\pi\nu^2}\ \frac{\tilde{\omega}_1}{\tilde{\omega}_0}\ A(1,0) \tag{3.2}$$

where f is the oscillator strength (sometimes called the f-value) for the state and the subscripts 1 and 0 denote the upper and ground states, respectively. We have used 0,1 instead of a more general i,j notation to signify a resonance, where radiation is resonantly scattered in the transition 1→0. The other symbols have their usual meanings. Finally, the intensity of the scattered column emission (in rayleighs) along the line of sight is

$$4\pi I = \int_{z_o}^{\infty} n(z)\ [\pi F_\nu(z)]\ \frac{\pi e^2}{m_e c}\ f(0,1)\ dz \tag{3.3}$$

This is the simplest form of the scattering equation.

To allow for deactivation as mentioned above, we can multiply the term under the integral in equation (3.3) by an effective albedo term which accounts for the ratio of transition probabilities, or

$$\tilde{\omega}(1,0) = \frac{A(1,0)}{A(1,0) + \eta(1,0)\ [X]} \tag{3.4}$$

Here, η is the rate coefficient for collisional deactivation of the (0,1) state, or simply the collision frequency, and [X] is the concentration of all non-(0,1) species, which is also a function of altitude. For unattenuated solar radiation, it is common practice to collect most of the terms of equation (3.3) into a constant for the particular state of the atom. Representing this constant as the so-called "g-factor" we have

$$4\pi I = g(0,1)\ n_{tot} \tag{3.5}$$

where n_{tot} represents the column density of the scatterers and g(0,1) is defined as

$$g(0,1) \triangleq \pi F_\nu(\infty)\ \frac{\pi e^2}{m_e c}\ f(0,1) \tag{3.6}$$

Thus, if we can measure the intensity of a particular resonance emission, we can find the integrated column density of the scatterers through their g-factors. The g-factors for various resonance lines of atoms and molecules have been computed and tabulated by Chamberlain [1961], Hunten [1967], and Gadsden [1969]. We repeat a table of the values (Table I) for some of the weaker features observed. It must be remembered that the value of g is found for unattenuated solar radiation. Modifications to the theory must be made when the radiation is partially absorbed or scattered by other atmospheric species before reaching the scattering volume [Swider, 1984]. These extra effects are illustrated in the next section.

Finally, the above treatment ignores two factors which may be important for certain types of radiations. The first is the optically thick atmosphere which effects the incident radiation. This adds an additional albedo term to the solar flux which splits the energy into absorbed and scattered components. It is unimportant, for example, for twilight metallic resonance observations as we show in an example below, but it could conceivably be important for corresponding dayglow measurements. The second effect is the polarization or anisotropy of the scattered radiation. This can be accounted for by adding a phase function to the scattered intensity equations given above as (3.3) and (3.5), where this phase function delineates the angular distribution of the scattered radiation. These extra effects have been detailed by Chamberlain [1978] and will not be repeated here.

Table I
Scattering Efficiencies for the Observed Species in Twilight

Species	Line(Å)	g(ph s^{-1})	Species	Line(Å)	g(ph s^{-1})
Fe	3860	0.014	Na D_2	5890	0.540
N_2^+ 1Neg	3914	0.050	Na D_1	5896	0.330
Ca^+ K	3934	0.270	Hα	6563	2.6×10^{-6}
Al	3962	0.041	Li	6708	8.7
Ca^+ H	3968	0.150	K D_1	7699	1.920
Mn	4031	0.037	O_2(0-1) Atm	8645	5.0×10^{-10}
Ca	4227	0.310	He(^{3}P)	10830	16.8
Cr	4254	0.037	O_2(0-0) IR Atm	12683	9.4×10^{-11}
N(^{2}D)	5200	7.5×10^{-11}	O_2(0-1) IR Atm	15803	1.2×10^{-11}

We now illustrate an example for an optically thin atmosphere. The absorption resonance scattering cross section is described by

$$\alpha_\nu = \frac{\pi e^2}{m_e c} f \frac{c}{V\nu\sqrt{\pi}} \exp\left[-\frac{c^2}{V^2}\frac{(\nu-\nu_o)^2}{\nu^2_o}\right] \text{ cm}^2 \qquad (3.7)$$

where the integrated absorption coefficient per atom per unit f-value is $\pi e^2/m_e c$ (=0.02647 $cm^2\ s^{-1}$, viz. equation 3.2), f is the oscillator strength, V is the thermal velocity ($\sqrt{2\kappa T/M}$) of the atoms of mass M, and ν_o is the center frequency [Chamberlain, 1961]. The other terms in the equation have their usual definitions. We next determine if the atmosphere is optically "thick" to an emission. Using the K line of the calcium ion as an example (at $\lambda = \lambda_o$ = 3934Å, f=0.69), and at T=200 K, the absorption coefficient is equal to 1.4×10^{-11} cm^2. This translates to a column abundance of about 7×10^{10} cm^{-2}. Using (3.5) and the appropriate g-factor from Table I, we see that for unit optical depth, the Ca^+ intensity must approach 19 kR. Measurements of the calcium ion intensity usually never exceeded 100 R, [Broadfoot, 1967; Tepley et al., 1981b], so, we can conclude that for this emission at least, the atmosphere is optically thin and as a result, the above equations for resonance scattering are valid.

Remember, the application of the g-factors in this way of course assumes that the excitation energy is only from direct solar flux. In actuality, this approach fails to account for the albedo of the atmosphere and reflections from the surface of the Earth, that is, backscattered radiation can excite resonances. For dayglow observations, the radiation due to the albedo is important as shown by McElroy and Hunten [1966], which leads to an increased excitation of the resonance energy resulting in an effective increase in the value of the g-factor. This would lower the determination of the column density of the scatterers. In twilight, however, when the excitation radiation originates from below the atmospheric region that is being observed, the albedo effects are

minimal, being overshadowed by such things as screening of the radiation in the lower atmosphere. The effects of albedo in twilight have been estimated for sodium by Chamberlain [1956] and Donahue et al. [1956] where they found that only a few percent correction should be applied.

4. TWILIGHT GEOMETRY

An optical twilight experiment is characterized by the sun being depressed a few, to a few tens of degrees below the horizon. During this time it is possible to obtain reasonable height information of the scatterers that could not otherwise be determined from nightglow work by recording the spectrum of the species with time resolutions of the order of ½° to 1° solar depression angle. Additionally, as the sun becomes depressed, much of the unwanted background intensity decays allowing for the detection of weaker emissions that cannot be seen in daytime.

Figure 3 illustrates the geometry encountered in twilight observations. We again follow the development given by Chamberlain [1961]. There are two important concepts which can be obtained from this figure, the geometrical shadow height and the screened shadow height. The latter is the result of extinction of the excitation radiation from the sun as it passes through the troposphere and stratosphere. This extinction is due to molecular (Rayleigh) scattering, and to the presence of ozone and aerosols which are responsible for absorption and scattering of the radiation. If we restrict observations to the plane of the solar azimuth, then from the figure we have six variables of interest. These are the angles α, β, γ, χ, θ, and height z_s. Here, α is defined as the solar depression angle with respect to the observer, and χ is the zenith angle of observations. Of these six parameters, only two are known, α and χ. For example, values of α can be calculated from knowledge of the solar declination, azimuth, and observational times.

The solution to the twilight problem requires four equations. Restricting the problem to an unscreened solar ray, from the triangle containing angle β in Figure 3, we have

$$z_s = Re(\sec\beta - 1) \tag{4.1}$$

where Re is the radius of the Earth. Using the law of sines for the triangle containing angle γ, we can define an equation used often in nightglow work, the van Rhijn equation,

$$\sin\theta = \frac{R_e}{R_e+z_s}\sin\chi = \cos\beta\sin\chi \tag{4.2}$$

We also have

$$\theta = \chi - \gamma \tag{4.3}$$

And finally, from the depression angle relationships

$$\sin\beta = \sin(\alpha-\gamma) = \sin\alpha\cos\gamma - \sin\gamma\cos\alpha \tag{4.4}$$

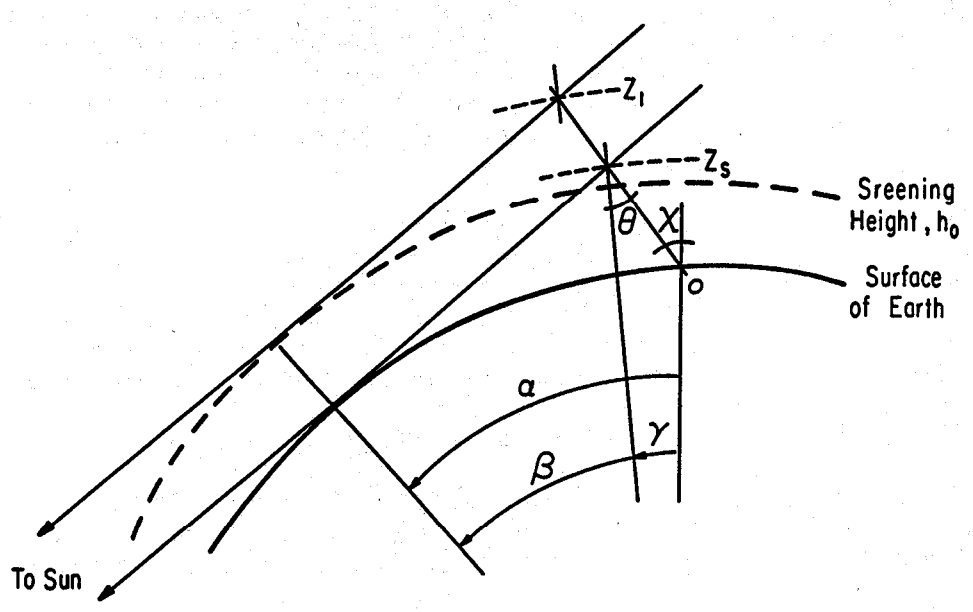

Figure 3 - The geometry encountered in twilight illustrating the screening of radiation from the sun by the lower atmosphere. The ray or line from the sun to Z_s grazes the solid earth and casts a shadow into the atmosphere at Z_s. The ray to Z_1 is the screened shadow line which "grazes" the screening height h_o. These shadow lines are not as distinct as pictured but are smeared in altitude (see text). The effects of refraction are also not shown. Observations from point O are made at a zenith angle χ; the other angles are described in the text. Generally, $\alpha \neq \beta + \gamma$ if the observations are not made in the plane of the sun's azimuth with respect to O [see Chamberlain, 1961].

When the observations are not in the plane of the solar azimuth, Chamberlain [1961] showed that equation (4.4) can be modified by including a factor, $\cos\phi$, multiplied by the last term, where ϕ is the azimuth angle between the sun and the observer. All of the other equations above remain the same. Additionally, for the simple case of zenith observations, $\alpha=\beta$ and $\theta=\gamma=\chi=0°$, only equation (4.1) remains. When the screening height h_o shown in Figure 3 is accounted for, then equation (4.1) becomes

$$z_1 = \mathrm{Re}\,(\sec\beta - 1) + h_o \sec\beta \qquad (4.5)$$

(For $h_o=0$, (4.5) reduces to (4.1) and $z_1=z_s$.) The other equations follow accordingly where, for the screened ray, γ increases while β decreases slightly, and α remains the same.

Finally, we should mention that the above analysis fails to account for the refraction of the incident solar ray. The actual ray would be bent toward the Earth by an amount

$$\Delta z \approx 127\,\frac{N(h_o)}{N(0)}\,\frac{\sin\beta}{\cos^2\beta} \qquad (4.6)$$

for $h_o << \mathrm{Re}$ and where N(z) is the total neutral density at altitude z. The factor 127 (=0.02 Re) has been measured from stellar occultations and applies for heights given in kilometers [Chamberlain, 1961]. For typical neutral concentrations, we find that refraction amounts to less than a 1% decrease in the shadow heights.

As a quick rule of thumb estimate, and neglecting proper dimensionality, we see that the height z_s in kilometers is approximately equal to the solar depression angle squared, that is, $z_s \approx \alpha^2$, where α is in degrees. If we include the atmospheric screening, then $z_1 \approx \alpha^2 + h_o$. These approximations appear to be good to 1-2% of the actual heights more rigorously calculated for the lower ionosphere.

4.1 Twilight screening and atmospheric transmission

The optical thickness of an atmosphere for a particular emission is related to the atmospheric transmission. In twilight when the shadow line is not sharply defined, then equation (3.5) must be modified by including a transmission function. Additionally, the screening height for a particular emission wavelength can be obtained from knowledge of the transmission of the lower atmosphere. The procedure has been outlined by Hunten [1962]. He used tables of molecular composition, ozone and dust concentrations, and accounted for refraction and the finite size of the sun. The resulting atmospheric transmission functions for various emissions, such as Na, Ca^+, and N_2^+, appeared somewhat Gaussian in shape having a mean value equal to the screening height and a standard deviation of one half the "smearing width" of the shadow line. No seasonal variations of the concentration of aerosols or ozone were taken into account which can alter the altitude of the screening height. In an attempt to account for the

uncertainties due to variations of atmospheric transmission, Tepley et al., [1981b] used additional information of the ionospheric structure determined from simultaneous electron density measurements and optical observations of Ca^+ in twilight. By assuming the calcium ions were distributed similarly to the electrons in layers, the electron density profile was then convolved with an atmospheric transmission function with zero screening and integrated with respect to altitude to simulate a column emission rate profile for the layered emitters. A comparison of the altitude distribution of the measured and synthesized optical profiles yielded the screening height.

The procedure is as follows. Referring to Figure 4 adopted from Hunten [1962], the observed emission $4\pi I(z_1)$ is the convolution of density n(z) and the transmission function $T(z-z_1)$,

$$4\pi I(z_1) = g \int_o^\infty n(z)T(z-z_1)\, dz \tag{4.7}$$

where g is the efficiency factor for resonant scattering mentioned previously. Equation (4.7) is a variation of (3.5) where z_1 is the screened shadow height. As shown in Figure 4, if we assume a Gaussian shape for the derivative of T with respect to z_1, then T is defined as the distribution function of the Gaussian probability density with zero mean,

$$T(z-z_1) \triangleq F(z_1) = \frac{1}{\sigma\sqrt{\pi}} \int_{-\infty}^{z_1} \exp\{-x^2/2\sigma^2\}\, dx \tag{4.8}$$

or

$$F(z_1) = \tfrac{1}{2}\,[1+\mathrm{erf}(z_1/\sigma\sqrt{2})] \tag{4.9}$$

where we have made use of the relationship between the integral of the Gaussian distribution and the standard error function which facilitates encoding into a computer program. After a suitable background density is removed, $F(z_1)$ is then convolved with a trial n(z) and the result is integrated numerically throughout the region where the emitters would be distributed.

5. TWILIGHT SPECTRAL DATA ANALYSIS

In this section we present a mathematical representation for the analysis of optical spectra measured during twilight. In order to obtain accurate values of any line emissions, all continua such as the scattered solar Fraunhofer structure, must first be removed. The technique is particularly useful for its application to weak twilight emissions such as resonance scattering from metallic species. The measured radiance during any given twilight period is composed of the solar and nightglow continua, the spectral distribution of line emissions, a quasi-continuum which may be the result of some fluorescent scattering mechanism, and instrumental noise. The relative distribution of these individual components might be used to infer the amount of fluorescence scattering, possibly due to aerosols within the atmosphere. In a later section we suggest

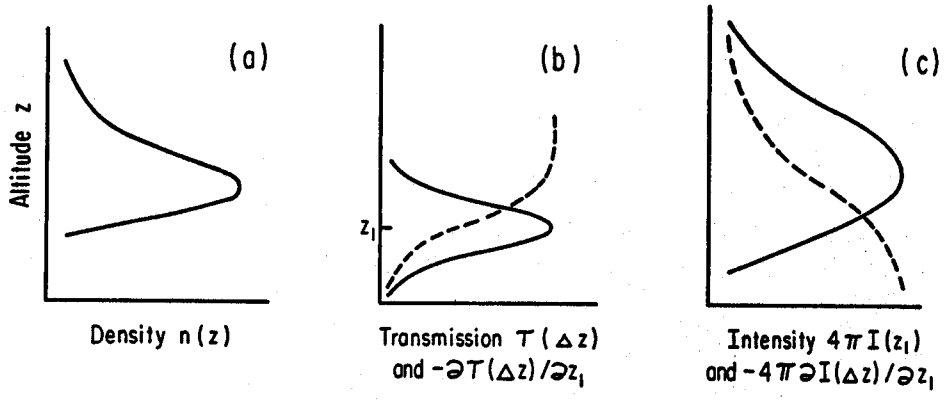

Figure 4 - The relationship between atmospheric transmission and the intensity measured from the distribution of the scatterers. The curve in panel (a) illustrates the altitude distribution of the scatterers. This curve also denotes their volume emission rate. The moving shadow line is represented by $T(\Delta z)$, where $\Delta z = z - z_1$, and is illustrated by a dashed line in (b) and its derivative is assumed to be a Gaussian (see text). The corresponding integrated intensities $4\pi I(\Delta z)$ and $-4\pi\partial I(\Delta z)/\partial z_1$, the dashed and solid curves in panel (c), respectively, are the convolutions of n(z) and their respective transmission functions. If the shadow line were sharply defined, then T would be a step function and ∂T a delta function at z_1. For that case, ∂I would have the same shape as n(z) with altitude [see Hunten, 1967].

a method by which this inference might be accomplished.

We call the analysis method the ratio algorithm. Another technique used to analyze twilight spectra involves scaling the solar continuum and subtracting it from the twilight spectra. That technique (call it "differencing") has met with some experimental success [Broadfoot and Hunten, 1966; Broadfoot, 1967] but cannot adequately account for an atmospheric fluorescence component which varies in wavelength. We demonstrate how ratioing is superior to differencing in terms of minimizing the accumulation of error inherent in the data analysis procedure. The following development can also be found in Tepley et al. [1981a].

5.1 Data reduction technique

To illustrate the ratioing procedure, we define $S(\alpha_o,\lambda)$ and $F(\alpha_o,\lambda)$ to be the amplitudes of the scattered solar continuum and the fluorescence continuum, respectively, for the solar depression angle α_o. Referring to Figure 5, these two components are shown by curves (a) and (e). The amplitude of the line emission represented by the function $L(\alpha_o,\lambda)\delta(\lambda-\lambda_o)$ is small compared with the values of S and F. The wavelength variable and the line position are denoted by the quantities λ and λ_o, and $\delta(\lambda-\lambda_o)$ is the Dirac delta function.

We assume that the spectral variation for either continuum is small within the resolution of the measuring instrument, or $\Delta\lambda$. This allows us to ignore the necessity of convolving the spectral shape of $\Delta\lambda$ with the measured spectra in the development that we present below.

At α_o, the measured spectrum is written as

$$M(\alpha_o,\lambda) = S(\alpha_o,\lambda) + F(\alpha_o,\lambda) \tag{5.1}$$

At a time further into twilight at a solar depression angle α, the amplitude of the line emission L becomes a significant part of the spectrum as compared with the attenuated amplitudes of the scattered solar and fluorescence continua, defined by the scale factors, a and b, respectively. This later spectrum is represented as

$$M(\alpha,\lambda) = aS(\alpha_o,\lambda) + bF(\alpha_o,\lambda) + L(\alpha,\lambda)\delta(\lambda-\lambda_o) \tag{5.2}$$

To remove the effects of the wavelength structure of the scattered solar continuum and the fluorescent continuum from the measured spectrum, we follow the procedure of Noxon et al. [1979] as modified to treat the problem of fluorescence contamination. For each spectrum we introduced a function $C(\alpha,\lambda)$ that may vary linearly in wavelength which we use to modify the amplitude of the measured spectrum, equation (5.2), by subtraction. This resultant is then divided by the spectrum $M(\alpha_o,\lambda)$. Dropping the depression angle arguments but introducing a subscript "$_0$" to denote the spectrum measured at α_o, these ratios are then given by

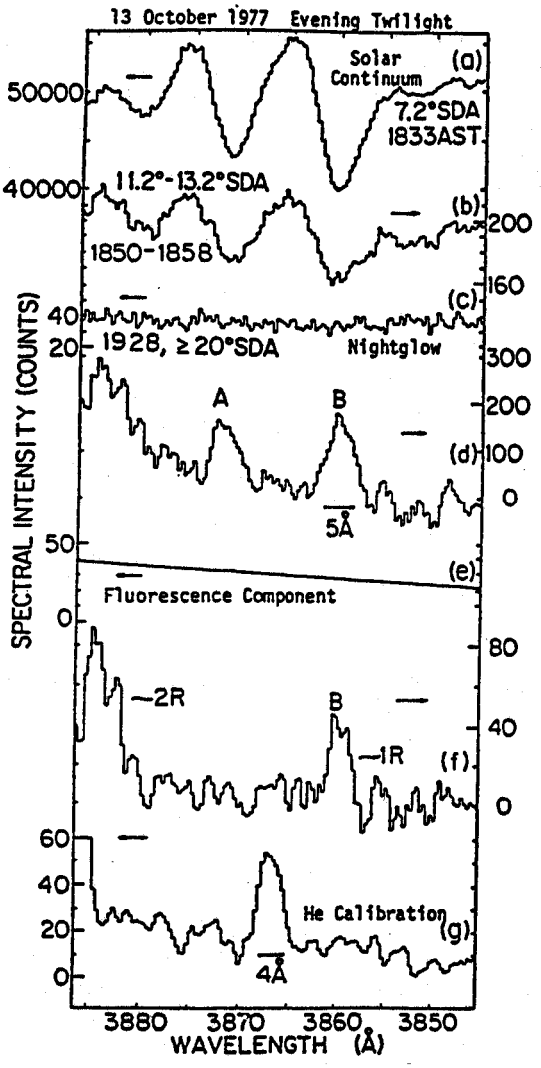

Figure 5 - An observation of neutral iron in twilight for 13 October 1977 illustrating the data reduction procedure. The measured solar continuum, middle twilight spectrum, and nightglow are shown by curves (a), (b), and (c), respectively. Spectrum (d) was obtained by subtracting only the nightglow from (b) and dividing by the solar continuum. The result is the appearance of false features A and B which are inversions of a residual continuum level in the Fraunhofer valleys. When an additional component with the trend given by (e) is also subtracted from (b) before it is ratioed with (a), then the result is shown in spectrum (f). The new feature B is attributed to the Fe resonance line at 3860Å having a width matching a He calibration line shown in the bottom curve. An additional feature in (f) at 3884Å is a portion of the R-branch of the N_2^+(1-1) 1st Negative band [see Tepley et al., 1981a].

$$\frac{M(\lambda) - C(\lambda)}{M_0(\lambda)} = \frac{aS_0(\lambda) + bF_0(\lambda) + L(\lambda)\delta(\lambda-\lambda_0) - C(\lambda)}{S_0(\lambda) + F_0(\lambda)} \tag{5.3}$$

Since the ratio F_0/S_0 is generally less than 5%, we can expand the function $S_0^{-1}[1+F_0/S_0]^{-1}$ in a binomial series and rewrite equation (5.3) as

$$\frac{M(\lambda) - C(\lambda)}{M_0(\lambda)} = a + \frac{1}{S_0(\lambda)}[(b - a)F_0(\lambda) - C(\lambda)] + \frac{L(\lambda_0)}{S_0(\lambda_0)}\left[1 - \frac{F_0(\lambda_0)}{S_0(\lambda_0)}\right] \tag{5.4}$$

where we have dropped terms of order S_0^{-2} which are negligible. If we chose C to be identical with $(b-a)F_0$, then equation (5.4) becomes linearly proportional to the line emission amplitude modified by the factor $(1 - F_0/S_0)$, which is close to unity. The wavelength variation of S_0^{-1} is small compared with the instrumental resolution $\Delta\lambda$ so that the line amplitude L can be extracted. To accomplish this, we remove the baseline "a" by subtraction and then multiply by $S_0(\lambda_0)$ to find the line amplitude.

The procedure, then, is to begin the processing with an assumed value for C, and then examine the resultant trial ratios for indications of Fraunhofer structure, which may be inverted if the trail value of C is too small (see Figure 5, curve d). After a number of iterations with different values for C, the processing is complete when the background signal is free of Fraunhofer structure and the width of any spectral line matches the width of the instrumental function as calibrated. These trial and error steps can be quite tedious. If large amounts of spectral data need to be processed routinely, it is best to automate the technique as demonstrated by Swift et al. [1988].

A couple of points about the behavior of the fluorescence component as a function of increasing solar depression angle are worth noting. If the scattered sunlight and the fluorescence decay together, then $b = a$ and $C = 0$, thus, S is proportional to F and it correctly represent the spectral shape of the fluorescence. The value of C required to produce the final result for solar depression angle α can increase as a function of α. If $C > 0$, then $b > a$ and this behavior reflects the fact that the fluorescence decays slower than the scattered light continuum which decreases exponentially at a rate determined by the neutral atmospheric scale height H. This represents a wide and uniform distribution of aerosols in the stratosphere and mesosphere having a scale height greater than H [Giovane et al., 1976]. On the other hand, the situation $C < 0$ is entirely possible. For this last case, $a > b$ and a fluorescence continuum which decreases faster than the scattered light demonstrates a sharper layering of aerosols with a scale height less than H, such as an accumulation of dust at the tropopause [Cadle and Grams, 1975].

The factors a and C are known from the processing. So $b = a + C/F_0$ gives the relative variation of the fluorescence. However, since the magnitude of F_0 is not known,

b cannot be determined as a function of time. Furthermore, the $(1 - F_0/S_0)$ correction to the line emission shown in equation (5.4) cannot be applied exactly since F_0 is unknown. Otherwise the emission is correctly determined. Finally, we note that this procedure is correct only if F_0/S_0 is much less than unity.

5.2 Examination of the behavior of fluorescence

For any given spectrum at time $t=t_i$, let $C(t_i)=C_i$, $b(t_i)=b_i$, and $a(t_i)=a_i$, where t_i represents the time at some solar depression angle α_i. At time t_o (that is, for α_o) we have the solar continuum measurement (see equation 5.1). Also at t_o we assume $a_o=b_o=1$, therefore, $C_o=0$.

We then have the relation at $t = t_i$,

$$C_i = (b_i - a_i)\, F_0 \tag{5.5}$$

described earlier, where a_i and C_i are known but b_i and F_0 are unknown. To attempt to determine these parameters exactly we need additional information. We know the shape of the curves describing C_i and a_i from the data processing (cf. Figure 6 in the next section) so the slope of these curves can be found. Differentiating C_i with respect to t_i yields

$$\frac{\partial C_i}{\partial t_i} = F_0 \left[\frac{\partial b_i}{\partial t_i} - \frac{\partial a_i}{\partial t_i} \right] \tag{5.6}$$

Partial derivatives are used since there is also a wavelength (λ) dependence. But if we are only concerned with a "short" spectral range in the vicinity of the emission line, then $\partial C_i/\partial\lambda = \partial b_i/\partial\lambda = \partial a_i/\partial\lambda = 0$ and we can replace the partials with total derivatives.

Next, we eliminate F_0 from equation (5.5) and (5.6) to obtain the differential equation for b_i,

$$\frac{db_i}{dt_i} - \left[\frac{1}{C_i} \frac{dC_i}{dt_i} \right] b_i + \left[\frac{a_i}{C_i} \frac{dC_i}{dt_i} - \frac{da_i}{dt_i} \right] = 0 \tag{5.7}$$

All terms in the brackets are known and can be considered constant at a specific time. However, to obtain a more general solution we must allow C and a to vary with time.

Holding the bracketed terms of equation (5.7) constant at $t=t_i$ we can rearrange the equation to attempt a solution,

$$\frac{d}{dt_i}(b_i - a_i) - \left[\frac{1}{C_i} \frac{dC_i}{dt_i} \right] (b_i - a_i) = 0 \tag{5.8}$$

Letting $\xi_i = b_i - a_i$, we can separate the variables of equation (5.8) to produce

$$\frac{1}{\xi_i} \frac{d\xi_i}{dt_i} = \frac{1}{C_i} \frac{dC_i}{dt_i} = K_i \tag{5.9}$$

where K_1 is the separation constant. This equation simply states that the slope of b-a divided by its magnitude is equal to the rate of change of C divided by its own magnitude at time $t = t_i$, within an arbitrary constant K_1. A quasi-solution to (5.9) might look like

$$\xi_i = (b_i - a_i) = C_i e^{K_1} = C_i K_2 \qquad (5.10)$$

where a new constant absorbs K_1 plus the integration constants produced from equation (5.9). Comparing equation (5.10) and (5.5) simply shows that $F_0=K_2^{-1}$ is a constant which we have assumed in the analysis.

One may think that it might be an easy task to determine this "constant of fluorescence" from the time variations of a_i and C_i by solving simultaneous equations generated at each time t_i. However, for times $t=t_1, t_2,...$, we have the unknown F_0 plus new unknowns b_i, that is, $b_1, b_2,...$ As a result we always have more unknowns than equations that can be formed. Even at $t=t_o$, $a_o=b_o=1$, but $C_o=0$ so K_2 (or F_0) cannot be determined by this method.

The only alternative is to obtain an accurate measurement of F_0 before each twilight experiment. This can be accomplished by viewing the depth of a solar Fraunhofer absorption feature directly by pointing the instrument at the sun, exercising appropriate care, of course. (Direct sunlight is necessary since the use of a diffuser or a white cardboard to reflect light into the instrument will produce an unwanted additional fluorescence of the diffusing material.) After a measurement of the sun is accomplished, point the instrument at the atmosphere near but away from the sun and remeasure the depth of the absorption valley. The percentage difference of the two valleys yields the value of the fluorescence parameter F_0. Using this F_0 and the subsequent variations of a_i and C_i in the twilight analysis, will allow for the determination of b_i, that is, the distribution of the fluorescence with time and corresponding altitude.

5.3 Error accumulation for the difference and ratio methods

We have mentioned that a ratio algorithm is superior to differencing in reducing the errors involved. For differencing, the choice of a small wavelength region (or a single point) for spectral normalization of the solar structure can be a source of large error. This error can be minimized by selecting additional normalization channels and finding the average of the supplementary reduced spectra. We have essentially done this with the ratio technique by taking into account every point in the spectrum when we do the division, that is, the entire spectrum is treated as a single unit.

To illustrate the errors involved in the two methods consider twilight spectral measurements M(t) having error $\Delta M(t)$. We will use t_o to represent the time of measurement of an early twilight spectrum composed mostly of the solar continuum (such as equation 5.1) and t_i to stand for other measurement times during intermediate twilight periods (say, > 5° or 6° solar depression). The difference algorithm uses a scale factor ε ($<<1$) applied to the solar structure to remove it by subtraction or

$$M(t_1) \pm \Delta M(t_1) - \varepsilon[M(t_0) \pm \Delta M(t_0)] \tag{5.11}$$

The upper bound of the error is found by making the difference in equation (5.11) as large as possible, or

$$M(t_1) - \varepsilon M(t_0) + [\Delta M(t_1) + \varepsilon \Delta M(t_0)] \tag{5.12}$$

The expression in brackets is the absolute error of the difference. The relative error in this case is the ratio of the absolute error to the magnitude of the difference. If the errors are small compared with the estimate of the measurement (i.e., $\Delta M << M$) then the relative error is given as

$$\frac{\Delta M(t_1) + \varepsilon \Delta M(t_0)}{|M(t_1) - \varepsilon M(t_0)|} =$$

$$\frac{M(t_1)}{|M(t_1) - \varepsilon M(t_0)|}\left(\frac{\Delta M(t_1)}{M(t_1)}\right) + \frac{\varepsilon M(t_0)}{|M(t_1) - \varepsilon M(t_0)|}\left(\frac{\Delta M(t_0)}{M(t_0)}\right) \tag{5.13}$$

The terms in the large parenthesis are the relative errors of each component. Each relative error is divided by the weighing factor $|M(t_1) - \varepsilon M(t_o)|$ so that the total relative error is not simply the sum of the individual errors. The error can become large since ε is ideally chosen to allow $\varepsilon M(t_o) \approx M(t_1)$ during data reduction.

In the ratio technique, the upper bound for the error which is similar to equation (5.12) is

$$\frac{M(t_1) + \Delta M(t_1)}{M(t_0) - \Delta M(t_0)} \tag{5.14}$$

We can rationalize this expression, neglect terms of order $(\Delta M)^2$, and rearrange to obtain

$$\frac{M(t_1)}{M(t_0)} + \underline{\frac{M(t_1)}{M(t_0)}\left[\frac{\Delta M(t_0)}{M(t_0)} + \frac{\Delta M(t_1)}{M(t_1)}\right]} \tag{5.15}$$

where we have underlined the absolute error of the quotient. The relative error is the underlined term divided by the magnitude of the quotient which, for the case of small errors, is simply the expression in brackets.

Now to simplify the expressions, we let $M(t_i)$ be represented by M_i (i=0,1) and $\Delta M_i = \Delta M(t_i) = \sigma$ where the errors σ are assumed to be equal for all spectra. The validity of this assumption is not critical for what we develop below. The ideal value for ε in the difference algorithm is M_1/M_o, so the absolute error for differencing (equation 5.12) becomes

$$D = \left[\frac{M_0 + M_1}{M_0}\right]\sigma \tag{5.16}$$

But, for the ratio method the absolute error is written as

$$R = \left[\frac{M_0 + M_1}{M_0^2}\right]\sigma \qquad (5.17)$$

so that the ratio of errors of the two methods is related to the magnitude of the solar continuum, that is, $D/R=M_o$. We note that this is true for all values of ε where $0 < \varepsilon < 1$ because $|M_1| < |M_o|$.

Finally, even though the relative error may not be an adequate representation of the true errors involved, the presence of the pole in the equation generated by the choice of the factor ε at some spectral elements indicates that the absolute errors can become large. On the other hand, there are no poles in the relative error of the ratio method which indicates that the absolute errors are stable. In light of these facts we see that the ratio technique is far superior to the method of differencing in minimizing the errors characteristic of the data analysis.

6. DISCUSSION

In the previous section we suggested that a measurement of a time sequence of optical twilight spectra might contain information about the distribution of aerosols. The amount of correction that is applied to remove the contaminating effects of aerosol fluorescence has a characteristic temporal and wavelength distribution different from the Rayleigh scattered solar continuum. By examining each spectral contribution from middle twilight where the fluorescence component is significant, and the rate at which the magnitudes of these components decay as the solar depression angle increases, a relative scale height might be obtained for the responsible contaminating mechanism or species.

A parameter that can represent the amount of atmospheric fluorescence continuum is the relative amplitude of the required correction with respect to the magnitude of the midtwilight spectra at the wavelength position of a particular resonance line. This signal level can be between a few percent and about 20% of the amplitude of midtwilight spectra. The time progression of the amplitude for the correction generally decreases at a rate less than the solar continuum. For example, in Figure 6 we show a few representative cases of the fluorescence correction amplitude plotted as a function of solar depression angle. These results were derived from several attempts to measure various metallic species of the lower ionosphere during a number of twilight periods at Arecibo. Shown are amplitude plots for different wavelengths. We can obtain some information on the degree of fluorescence even though an emission line is not present in the spectrum. For example, no manganese emissions were ever detected at 4031Å. But the amount of correction required to "flatten" the midtwilight spectra, that is, by removing the solar Fraunhofer structure, can indicate the degree of atmospheric fluorescence near 4000Å.

We suggested that the fluorescence component arises from the presence of aerosols in the lower atmosphere. Basically aerosols can be described as mineral. The reader may have seen museum displays of minerals or meteorites fluoresce under ultraviolet light. The minerals absorb ultraviolet radiation and fluoresce at longer wavelengths.

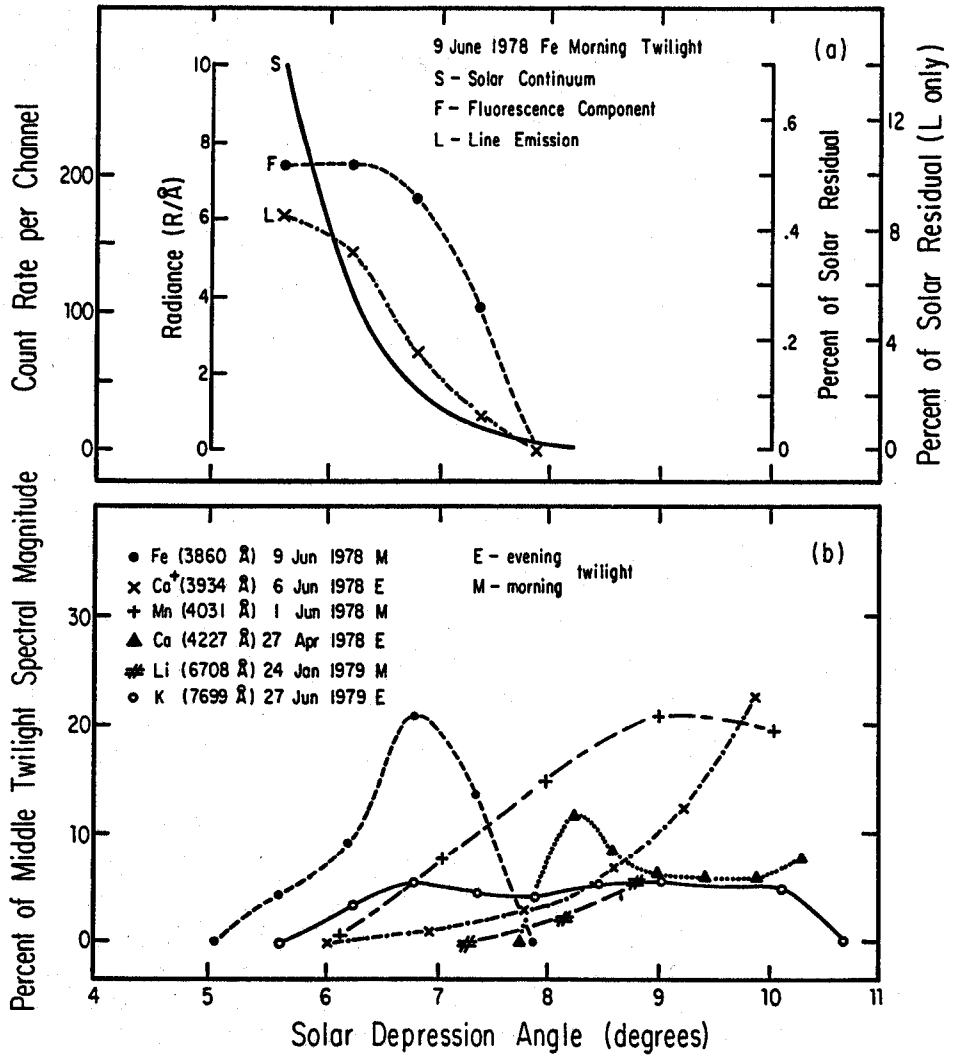

Figure 6 - The temporal variation of the magnitude of the fluorescence component for several wavelengths derived from optical twilight observations at Arecibo. The top panel illustrates the amplitude relationship between the three twilight components, S, F, and L, with respect to the residual level of the solar Fraunhofer absorption (c.f. equation 5.2 in the text) for an Fe observation during a morning twilight [see Tepley et al., 1981a]. Panel (b) shows the relative percentage of the fluorescence component with respect to the magnitudes of the middle twilight spectra which are required to produce flat and featureless spectra, that is, without inverted or non-inverted Fraunhofer absorptions. These results, as a function of solar depression angle, indicate a greater degree of fluorescence in the blue than in the red portions of the spectrum.

Fluorescence is observed in the near UV, blue, and green portions of the spectrum while very few emissions are observed in red. We see from Figure 6 that most results are near the blue portion of the spectrum. But, by comparing the Ca^+ and Fe results to the Li and K fluorescence profiles, there appears to be a greater degree of fluorescence in the blue than in the red, at least qualitatively. We should mention that these data do not adequately cover the expected seasonal effects inherent in the implied aerosol fluorescence. We will discuss these aspects further.

In twilight data analysis we have stressed the need to account for the continuum resulting from the fluorescence of aerosols which are bathed in direct solar or scattered radiation. These aerosols are in the form of dust, NO_2, or pollutants found in the stratosphere and troposphere. The concentrations of aerosols may be low but the amount of scattering in the lower atmosphere is high [Kompaniets, 1965]. The continuum emitted by aerosols when illuminated by the sun will always contain a small fraction of the scattered solar continuum. If the relative fraction of the background continuum due to fluorescence were to remain constant throughout twilight, then the Fraunhofer structure can be removed by either scaling and subtraction [Broadfoot, 1967] or rationing [Noxon et al., 1979]. Furthermore, as the example of Figure 6 illustrated, if the decrease in the amplitude of the fluorescence continuum as a function of solar depression angle is less than the decrease in the scattered solar continuum, then this behavior indicates that the scale height for the distribution of aerosols is greater than the atmospheric scale height. This is expected if the concentrations of aerosols in the stratosphere (and mesosphere) are in the form of broad layers or wide distributions [Rosen, 1969; Link, 1973]. The differencing technique used to remove Fraunhofer structure assumes that the relative intensity distribution of the background continuum will not vary throughout twilight. When the fluorescence decays at a different rate than the scattered light continuum, and it is not taken into account, the effect of normalization by scaling can produce an enhanced emission rate of an airglow line.

We estimate that what we call the fluorescence component of twilight is very similar (if not identical) to the Ring effect found in dayglow observations [Grainger and Ring, 1962; Hunten, 1970; Chanin, 1975]. These studies attributed the Ring effect to albedo changes during solar transit or to rotational Raman scattering of molecules such as N_2 and O_2 [Brinkmann, 1968; Noxon et al., 1979]. The percentage of this scattering has been measured to usually increase or remain constant with increasing solar zenith angle. Barmore [1975] however, reported both increasing and decreasing scattering as the solar zenith angle increased using high resolution dayglow measurements of the 6300Å Fraunhofer absorption line. He was able to eliminate other possible mechanisms for the scattering as being of little significance, and concluded that the variations observed were due to random variations in the amount of fluorescing material. For example, the surface of the Earth does indeed fluoresce and this may be important when the atmospheric turbidity is low. However, the presence of the Ring effect after sunset indicates that there is a fluorescence in the stratosphere. Kattawar et al. [1981] on the other hand, favor Brinkmann's proposed mechanism for the filling-in of Fraunhofer lines and extended the theory to include inelastic Rayleigh-Brillouin scattering together with

rotational Raman scattering.

From observations at low latitudes we have found that the magnitude of the fluorescence component of twilight spectra is variable from day to day displaying both increasing and decreasing trends with increasing solar depression angle. Its relative magnitude was observed to vary by as much as 20% within a single twilight. There is also a great variability in the dust and aerosol concentrations with geographic location, in particular for the lower latitudes [Prospero et al., 1970; Carlson and Prospero, 1972]. Because of this daily variability of aerosols, it is also unwise to use the solar continuum from one twilight to reduce the spectra of another twilight, even though care is maintained to set up identical experimental conditions. However, by applying proper data analysis procedures as outlined in this report, the measurement of weak emissions during twilight can contribute a great deal to the understanding of atmospheric composition and the relative distribution of aerosols in the middle and lower atmosphere.

ACKNOWLEDGEMENTS

I am very grateful to Ms. Carmen Torres for her proficiency and patience during the preparation of this report. I would also like to thank Dr. Doug Torr for allowing me to present some of the work of his group (figure 1) before publication. Results shown in some of the other figures were from observations at the Arecibo Observatory which is operated by Cornell University under a cooperative agreement with the National Science Foundation.

REFERENCES

Barbier, D., Recherches sur la raie 6300 de la luminescence atmosphérique nocturne, *Ann. Geophys., 15,* 179-217, 1959.

Barmore, F. E., The filling-in of Fraunhofer lines in the day sky, *J. Atmos. Sci., 32,* 1489-1493, 1975.

Brinkmann, R. T., Rotational Raman scattering in planetary atmospheres, *Astrophys. J., 154,* 1087-1093, 1968.

Broadfoot, A. L., Twilight Ca^+ emission from meteor trails up to 280 km, *Planet. Space Sci., 15,* 503-514, 1967.

Broadfoot, A. L., and A. E. Johanson, Fe(3860Å) emission in the twilight, *J. Geophys. Res., 81,* 1331-1334, 1976.

Broadfoot, A. L., and D.M. Hunten, N_2^+ emission in the twilight, *Planet. Space Sci., 14,* 1303-1319, 1966.

Brown, T. L., The chemistry of metallic elements in the ionosphere and mesosphere, *Chem. Rev., 73,* 645-667, 1973.

Cadle, R. D., and G. W. Grams, Stratospheric aerosol particles and their optical properties, *Rev. Geophys. Space Phys., 13,* 475-501, 1975.

Carlson, T. N., and J. M. Prospero, The large-scale movement of Saharan air outbreaks over the northern equatorial Atlantic, *J. Appl. Meteor, 11,* 283-297, 1972.

Chamberlain, J. W., Resonance scattering by atmospheric sodium-I Theory of the intensity plateau in the twilight airglow, *J. Atmos. Terr. Phys., 9,* 73-89, 1956.

Chamberlain, J. W., *Physics of the Aurora and Airglow,* Academic Press, New York, NY, 1961.

Chamberlain, J. W., *Theory of Planetary Atmospheres: An Introduction to Their Physics and Chemistry,* 1st edition, Academic Press, New York, NY, 1978.

Chanin, M. L., Filling in of the Fraunhofer lines by scattering on the ground, *J. Geophys. Res., 80,* 2859-2862, 1975.

Clemesha, B. R., Lidar studies of the alkali metals, MAP Handbook, *13,* 99-112, 1984.

Donahue, T. M., R. Resnick, and V. R. Stull, Distribution in the upper atmosphere of sodium atoms excited by sunlight, *Phys. Rev., 104,* 873-879, 1956.

Dufay, M., Étude de l'emission de la molécule d'azote ionisée et de l'atome neutre d'azote au crépuscule, *Ann. Phys., 8,* 813-862, 1959.

Evans, W. F. J., and E. J. Llewellyn, Measurements of mesospheric ozone from observations of the 1.27μ band, *Radio Sci., 7,* 45-50, 1972.

Evans, W. F. J., H. C. Wood, and E. J. Llewellyn, Ground-based photometric observations of the 1.27μ band of O_2 in the twilight airglow, *Planet. Space Sci., 18,* 1065-1073, 1970.

Fedorova, N. I., On emission λ 10830Å in aurorae, *Planet. Space Sci., 5,* 75, 1961.

Fricke, K. H., and U. von Zahn, Mesopause temperatures derived from probing the hyperfine structure of the D_2 resonance line of sodium by lidar, *J. Atmos. Terr. Phys., 47,* 499-512, 1985.

Gadsden, M., Antarctic twilight observations, I. Search for metallic emission lines, *Ann. Geophys., 25,* 667-677, 1969.

Gardner, C. S., and J. D. Shelton, Density response of neutral atmospheric layers to gravity wave perturbations, *J. Geophys. Res., 90,* 1745-1754, 1985.

Giovane, F., D. W. Schuerman, and J. M. Greenberg, The solar occultation technique for remote sensing of particulates in the Earth's atmosphere, 2. Skylab results of a 48-km aerosol layer, *J. Geophys. Res., 81,* 5383-5388, 1976.

Grainger, J. F., and J. Ring, Anomalous Fraunhofer line profiles, *Nature, 193,* 762, 1962.

Granier, C., J. P. Jegou, and G. Megie, Iron atoms and metallic species in the Earth's upper atmosphere, *Geophys. Res. Lett., 16,* 243-246, 1989a.

Granier, C., J. P. Jegou, and G. Megie, Atomic and ionic calcium in the Earth's upper atmosphere, *J. Geophys. Res.,* in press, 1989b.

Granier, C., and G. Megie, Daytime lidar measurements of the mesospheric sodium layer, *Planet. Space Sci., 30,* 169-177, 1982.

Henriksen, K., G. G. Sivjee, and C. S. Deehr, Winter enhancement of atomic lithium and sodium in the polar upper atmosphere, *J. Geophys. Res., 85,* 5153-5156, 1980.

Hunten, D. M., Transmission functions for twilight studies, *J. Atmos. Terr. Phys., 24,*333-338, 1962.

Hunten, D. M., Spectroscopic studies of the twilight airglow, *Space Sci. Revs., 6,* 493-573, 1967.

Hunten, D. M., Surface albedo and the filling-in of Fraunhofer lines in the day sky, *Astrophys. J., 159,* 1107-1110, 1970.

Kattawar, G. W., A. T. Young, and T. J. Humphreys, Inelastic scattering in planetary atmospheres, 1. The ring effect with aerosols, *Astrophys. J., 243,* 1049-1057, 1981.

Kirchhoff, V. W. J. H., and B. R. Clemesha, Atmospheric sodium measurements at 23°S, *J. Atmos. Terr. Phys., 35,* 1493-1498, 1973.

Kompaniets, A. I., Aerosol light scattering indicatrices in the free atmosphere at heights of the order of 10 km, *Izv. Atmos. Oceanic Phys., 1,* 335-338, 1965.

Kwon, K. H., C. S. Gardner, D. C. Senft, F. L. Roesler, and J. Harlander, Daytime lidar measurements of the tidal winds in the mesospheric sodium layer at Urbana, Illinois, *J. Geophys. Res., 92,* 8781-8786, 1987.

Link, F., Aerosols and particles, in *Physics and Chemistry of Upper Atmospheres,* B. M. McCormac, ed. D. Reidel, Dordrecht, Holland, pp. 34-40, 1973.

Lowe, R. P., K. L. Gilbert, and R. J. Niciejewski, Twilight intensity variation of the infrared hydroxyl airglow, MAP Handbook, *10,* 176-178, 1984.

Lytle, E. A., and D. M. Hunten, Observations of N_2^+ twilight and sunlit aurora, *Can. J. Phys., 40,* 1370-1384, 1962.

McElroy, M. C., and D. M. Hunten, A method of estimating the Earth albedo for dayglow measurements, *J. Geophys. Res., 71,* 3635-3638, 1966.

Megie, G., F. Bos, J. E. Blamont, and M. L. Chanin, Simultaneous nighttime lidar measurements of atmospheric sodium and potassium, *Planet. Space Sci., 26,* 27-35, 1978.

Meriwether, J. W., Jr., D.G. Torr, J. C. G. Walker, and A. O. Nier, The $O^+(^2P)$ emission at 7320Å in twilight, *J. Geophys. Res., 83,* 3311-3319, 1978.

Meriwether, J. W., Jr., Measurement of weak airglow emissions with a scanning spectrometer, *Planet. Space Sci., 27,* 1221-1232, 1979.

Noxon, J.F., Twilight enhancement in $O_2(b^1\Sigma_g)$ airglow emission, *J. Geophys. Res., 80,* 1370-1373, 1975.

Noxon, J. F., E. D. Whipple, and R. S. Hyde, Stratospheric NO_2, 1. Observational methods and behavior at mid-latitude, *J. Geophys. Res., 84,* 5047-5065, 1979.

Noxon, J. F., A study of the 6300Å oxygen line in the day airglow, *J. Geophys. Res., 69,* 3245-3255, 1964.

Pick, D. R., E. J. Llewellyn, and A. Vallance Jones, Twilight airglow measurements of the OH and O_2 bands by means of balloon-borne instruments, *Can. J. Phys., 49,* 897-905, 1971.

Prospero, J. M., E. Bonatti, C. Schubert, and T. N. Carlson, Dust in the Caribbean atmosphere traced to an African dust storm, *Earth Planetary Sci. Lett., 9,* 287-293, 1970.

Rosen, J. M., Stratospheric dust and its relationship to the meteoric influx, *Space Sci. Res., 9,* 58-59, 1969.

Swider, W., Ionic and neutral concentrations of Mg and Fe near 92 km, *Planet. Space Sci., 32,* 307-312, 1984.

Swift, W., D. G. Torr, M. R. Torr, C. Hamilton, and P. Bhatt, Spectral extraction from twilight airglow, paper at 1988 CEDAR Summer Workshop, Boulder, CO, 1988.

Tepley, C. A., J. W. Meriwether, Jr., J. C. G. Walker, and J. D. Mathews, Observations of neutral iron emission in twilight spectra, *J. Geophys. Res., 86,* 4831-4835, 1981a.

Tepley, C. A., J. D. Mathews, J. W. Meriwether, Jr., and J. C. G. Walker, Observations of the Ca^+ twilight airglow from intermediate layers of ionization, *J. Geophys. Res., 86,* 7781-7786, 1981b.

Torr, D. G., M. R. Torr, J. W. Meriwether, Jr., and R. G. Burnside, Measurements of the metastable $N^+(^1S)$ 5755Å emission in the twilight thermosphere, *J. Geophys. Res., 86,* 2314-2316, 1981.

Torr, D. G., W. A. Abdou, M. R. Torr, R. G. Burnside, and J. W. Meriwether, Jr., Measurements of the metastable $N^+(^1D)$ 6584Å emission in the twilight thermosphere, *J. Geophys. Res.*, *88*, 3190-3196, 1983.

Torr, M. R., D. G. Torr, P. Bhatt, W. Swift, and H. Dougani, Ca^+ emission in the sunlit ionosphere, *J. Geophys. Res.*, in press, 1989.

Vallance Jones, A., and A. W. Harrison, Calcium and oxygen in the twilight airglow, *Ann. Geophys.*, *14*, 179-185, 1958.

von Zahn, U., and R. Neuber, Thermal structure of the high latitude mesopause region in winter, *Beitr. Phys. Atmosph.*, *60*, 294-304, 1987.